Stochastic Environmental Research and Risk Assessment (2026) 40:78
https://doi.org/10.1007/s00477-026-03204-3

ORIGINAL PAPER

Spatial persistence in the Brahmaputra river: rescaled range and multiscaling analyses

Samuele De Bartolo[1] · **Carlo De Michele**[2] · **Leonardo Primavera**[3]

Received: 17 September 2025 / Accepted: 26 February 2026 / Published online: 1 April 2026

Abstract

Braided channel networks (BCNs) are highly dynamic fluvial systems characterized by multiple interweaving channels, whose configurations emerge from complex interactions between sediment transport and flow dynamics. This study proposes a novel methodological framework to analyze the scaling behavior of the braiding index N_{wc}, defined as the number of active wet channels within a given river reach. The approach integrates Rescaled Range (R/S) analysis with a fixed-size multifractal formalism, grounded in the Multifractal Detrended Fluctuation Analysis (MF-DFA) technique, to simultaneously capture long-range spatial dependence and multifractal scaling properties. The methodology is applied to 12 spatial datasets of the Brahmaputra River, derived from multisource satellite imagery spanning more than three decades and multiple spatial resolutions. Our results reveal a clear tendenc y toward persistence in the spatial organization of N_{wc}, as indicated by Hurst exponents consistently exceeding 0.5. This indicates the presence of significant long-range spatial correlations in the structure of BCNs. Furthermore, the stability of the multifractal spectrum widths, $\Delta\alpha$, across all datasets highlights the presence of intrinsic self-organizing processes governing the braided river morphology, providing new insights into the scaling of complex fluvial systems.

1 Introduction

Braided channel networks (BCNs) are intricate fluvial systems composed of multiple interlaced channels that repeatedly diverge and converge around sediment bars or mid-channel islands. These networks typically develop in geomorphic settings characterized by high sediment supply and variable discharge regimes, such as: i) glacial outwash plains, where meltwater rivers transport abundant sediment from retreating glaciers; ii) alluvial fans at mountain fronts, where flow deceleration leads to sediment deposition and channel splitting; iii) steep mountain rivers with coarse bedload and dynamic flow conditions; and iv) arid or semi-arid regions, where episodic but intense precipitation generates highly variable, short-lived flow events. In contrast to meandering systems, BCNs exhibit persistent morphological reorganization and rapid channel shifting, which make them suitable natural laboratories for investigating non-linear dynamics and scale-dependent processes in fluvial systems Ashmore (2013); Ashmore (2009); Bristow and Best (1993); Paola et al. (1996); Hundey and Ashmore (2009); Castelltort (2018).

Over the past two decades, significant efforts have been devoted to uncovering the scaling laws and multiscaling features of braided channel networks (BCNs). Prior studies have revealed topological regularities, mono - and multifractal characteristics, and striking analogies with complex physical systems such as turbulence and superconductivity (Sapozhnikov and Foufoula-Georgiou 1995, 1996, 1997; Sapozhnikov et al. 1998; Bassler and Paczuski 1998; Bassler et al. 1999; Walsh and Hicks 2002; Foufoula-Georgiou and Sapozhnikov 2001; De Bartolo et al. 2006, 2022; Stecca and Hicks 2022). More recently, second-order statistical approaches—such as Taylor's Power Law (TPL)—have been combined with multifractal analysis to explore the spatial variability of key geomorphic indicators, including the

✉ Samuele De Bartolo
samuele.debartolo@unisalento.it

[1] Department of Engineering for Innovation, EUropean Maritime Environmental Research (EUMER), University of Salento, via per Monteroni, S.P.6, 73100 Lecce, Italy

[2] Department of Civil and Environmental Engineering, Politecnico di Milano, Piazza Leonardo da Vinci 32, 20133 Milano, Italy

[3] Department of Physics, University of Calabria, via P. Bucci, 87036 Rende, Cosenza, Italy

number of active wet channels (N_{wc}), the average wetted width (w_{wc}), and the Entropic Braiding Index (EBI) (Taylor 1961, 2019; De Bartolo 2024; Rizzello et al. 2024). Notably, the work by Rizzello et al. (2024) has shed light on distinctive persistence patterns in N_{wc}, suggesting non-trivial long-range spatial correlations within the braided morphology. While these findings represent a valuable advancement in understanding BCN scaling, a more direct quantification of persistence–particularly through the lens of the Hurst exponent–remains an open and promising research direction. Essentially, these efforts have revealed non-trivial signatures of persistence and intermittency, suggesting the presence of long-range spatial correlations within the active channel network.

The objective of the present work is to provide robustness in the estimation of the Hurst exponent by employing two of the most widely recognized methodologies in the specialized literature: the Rescaled Range (*R*/*S*) Analysis (Hurst 1951; Mandelbrot 1982; Feder 1988), essentially based on simple (monofractal) scaling, and the Multifractal Detrended Fluctuation Analysis (MF-DFA) (Kantelhardt et al. 2001, 2002), which allows for a generalization of the Hurst exponent H to $H(q)$ (where q is the order of the fluctuation function) and enables the determination of the multifractal spectrum $f(\alpha)$. These methods are complementary: while *R*/*S* analysis offers a straightforward estimation of long-range dependence under monofractal assumptions, MF-DFA extends the analysis to capture scale-dependent fluctuations and heterogeneity in the scaling behavior, making it suitable for detecting multifractal features in complex spatial signals such as N_{wc}.

The analyses were applied to the Brahmaputra River. We acknowledge that the classification of the Brahmaputra River is not entirely unambiguous in the literature. According to Makaske (2001), Sarma (2005), Latrubesse (2008), Brahmaputra River is classified as an anastomosing river system with braiding occurring within individual channels. Other studies refer to the Brahmaputra as a braided river with some anastomosed regions (Best et al. 2022; Nandi et al. 2023; Nelson et al. 2025; Sarker and Thorne 2006), particularly when emphasizing its highly multi-thread planform, channel mobility, and bar-dominated morphology at certain spatial and temporal scales. For this, in the next, we adopt the term 'braided' in a functional sense, referring to the presence of multiple simultaneously active channels within a wide alluvial corridor, while recognizing that the Brahmaputra exhibits mixed braided–anastomosing characteristics depending on scale and hydrological conditions. The braided fluvial structures of Brahmaputra River were identified from satellite imagery at multiple spatial resolutions, over the period 1976–2007. The use of both *R*/*S* and MF-DFA analyses across such a diverse spatio-temporal dataset provides a robust framework for capturing the persistent and multifractal nature of river morphology.

2 Concepts and methods

2.1 Overview of analytical framework and previous investigations on N_{wc} scaling: the role of signal persistence

Braided channel networks (BCNs) have been increasingly examined through the lens of scaling laws and multifractal frameworks, with particular attention to the behavior of key geomorphic indicators. Among these, the number of active wet channels, denoted as N_{wc}, has emerged as a critical variable for capturing the spatial complexity of braided patterns. A precise definition of N_{wc} is provided in Sect. 2.2. In recent years, we have conducted a series of investigations aimed at quantifying the variability and scaling properties of N_{wc} using multifractal measures and second-order statistical tools such as Taylor's Power Law (TPL). A seminal contribution in this context is the work by De Bartolo et al. (2015), which investigated braided river systems observed in the *Fiumare* of Calabria, fluvial environments typical of southern Italy. These systems exhibit distinct seasonal behaviors; the streams are essentially ephemeral and characterized by highly variable discharge regimes. Through a direct simple-scaling analysis, the number of active wet channels in the Allaro *Fiumara* exhibited scale-invariant features over the spatial range of 5 to 100 meters. The probability distribution of active wet channels can be described using a power-law of the form:

$$P(N_{wc} \geq \mu) \sim a \cdot \mu^{b} \tag{1}$$

where P is the probability, a and b are the scale and shape parameters, respectively, and μ is the minimum value of active wet channels for braided systems ($\mu > 1$). In this formulation, the spatial partition Δs determines the resolution and the river sections used to calculate $P(N_{wc} \geq \mu)$, even if, it does not explicitly appear in the power-law expression. These results were both preliminary and encouraging, motivating the extension of the analysis to additional datasets by generalizing the probabilistic framework through a second-order theory based on variance, known as Taylor's Power Law (TPL) (Taylor 1961, 2019). The 2022 work by De Bartolo et al. (2022) can be regarded as the first application of this direct scaling methodology to the spatial variable N_{wc}. This work proved to be significant for two main reasons: first, it highlighted a deep interconnection between power-law behavior and the intermittent nature of the N_{wc} signals; second, it showed that the estimated scaling exponents

reflect a multiscaling support, thus indicating a multifractal nature. These results were consistent with findings from other contexts involving essentially geometric measures, evaluated within the net-points describing the planimetric shape of braided river systems (De Bartolo et al. 2006).

Further refinements in terms of Taylor's power laws (TPL) and multifractal measures were conducted by Rizzello et al. (2024) on various braided river structures, including those of the Rakaia River (New Zealand). They characterized the multifractal behavior of braided systems based on a generalized framework of the transformed TPL, developed according to the *Delta Method* (Taylor 2019), combined with an investigation using fixed-mass multifractal measures. These investigations also related the initial multifractal measures, in particular the singularities α, to the Hurst exponent, providing preliminary results that indicate a generally persistent behavior of the number of wet channels analyzed. Recently, alongside these studies, De Bartolo and De Michele (2025) and De Michele et al. (2025) provided further assessments. The former focused on direct scaling analyses by examining the behavior of braided systems within the framework of branching process theories (Harris 1989) and self-organized criticality (SOC) (Jensen 1998; Bak et al. 1987, 1988), while the latter introduced an analysis of the support of the N_{wc} measures using structure functions and fixed-mass multifractal methods. These investigations, once again, highlighted a direct correspondence between power laws - such as the one expressed in Eq. (1)—and those typically observed in self-organized criticality (SOC) processes (Bak et al. 1987, 1988), at least with reference to the braided network of the Brahmaputra River, which is a trans-boundary, large, sand-bed, mildly sloping braided river that flows from the Eastern Himalayas across the Bengal Basin to the Ganges-Brahmaputra-Meghna delta in the Bay of Bengal. The work by De Michele et al. (2025) has preliminarily addressed the relevance of deepening the investigation of Hurst exponents in relation to the multifractal spectra $f(\alpha)$. In this context, the authors thoroughly emphasized the importance of identifying the limitations imposed by the methodological foundations of direct multifractal analyses when estimating Hurst exponents, particularly with regard to the use of structure functions. Indeed, the use of generalized models for estimating the scaling exponents $\zeta(p)$ of structure functions may lead to underestimations of the Hurst exponent, potentially distorting the assessment of the persistent (or non-persistent) behavior of the N_{wc} signal. The preliminary results, although displaying an apparent local antipersistent behavior, are found to depend significantly on the application of corrective factors required for an accurate estimation of the scaling exponents $\zeta(p)$ (De Michele et al. 2025). This calls for a more in-depth investigation of multifractal measurement techniques, aimed at achieving a robust characterization of the scaling exponents and, in particular, of the Hurst exponent, which is generalized within this multiscaling framework.

Understanding the persistence or anti-persistence of the N_{wc} signal has direct geomorphological and hydraulic implications. A persistent signal, characterized by positive spatial correlations, suggests that an increase in the number of active channels in one river section is likely to be followed by a similar increase in downstream sections. This reflects morphological stability and coherence, often linked to relatively uniform flow conditions, sediment supply, and channel-forming processes, as well as strong lateral connectivity in fluvial dynamics. Conversely, an anti-persistent signal, marked by negative correlations, indicates high local variability and potential morphological instability: an increase in active channels in one section is typically followed by a decrease in the next, pointing to the influence of local hydraulic disturbances, sediment heterogeneity, or transitional morphodynamic phases.

From an applied perspective, analyzing the persistence properties of N_{wc} can help identify reaches of hydraulic stability versus zones undergoing active morphological change, supporting targeted river management strategies and improving morphodynamic predictions. Persistent reaches may exhibit predictable channel configurations over time, while anti-persistent reaches respond more strongly to short-term forcing. The Hurst exponent H provides a quantitative descriptor of these behaviors: values above 0.5 indicate long-range persistence, values below 0.5 indicate anti-persistence, and values around 0.5 indicate the absence of long-range dependence, though short-range correlations may still exist. Evaluating H in this context provides insight into the spatial organization of multi-thread channel networks, with direct implications for hydraulic modeling and sediment transport analysis.

2.2 Rescaled range (*R*/*S*) analysis

The *R*/*S* (Rescaled Range) analysis, proposed by Hurst (1951), is a statistical technique used to detect long-range dependence within time series or spatial data. Its purpose is to estimate the *Hurst exponent H*, which quantifies the degree of persistence or anti-persistence in the variability of the data. In the present study, the analysis is applied to a spatial series represented by the number of active wet channels observed along the longitudinal axis of a braided river, denoted by the function:

$$N_{wc}(x) : \mathbb{R} \rightarrow \mathbb{N} \tag{2}$$

where $N_{wc}(x)$ is a discrete variable consisting of non-negative integer values that represent the number of active wet

channels at the cross section located at position x. For each sampling point x_i, the value $N_{wc}(x_i)$ is measured, resulting in a discrete data sequence of $N_{wc}(x_1)$, $N_{wc}(x_2)$, , $N_{wc}(x_M)$ elements, where M denotes the total number of sampling points. This sequence is then used as input for the *R*/*S* analysis to estimate the spatial persistence and morphological complexity of the braided fluvial system. Therefore, let $\{x_1, x_2, \ldots, x_M\}$ be an ordered sequence of equally spaced spatial positions along the river course. To each x_i, the number of active channels $N_{wc}(x_i)$ is associated, yielding the discrete series:

$$\mathcal{N} = \{N_{wc}(x_1), N_{wc}(x_2), \ldots, N_{wc}(x_M)\}\,. \tag{3}$$

The series $\mathcal{N}$ is divided into k non-overlapping subsequences of length n, such that $M = k \cdot n$. Each subsequence, for $j = 1, 2, \ldots, k$, is defined as:

$$\mathcal{N}^{(j)} = \{N_{wc}(x_{j,1}), N_{wc}(x_{j,2}), \ldots, N_{wc}(x_{j,n})\}\,, \tag{4}$$

through which all the variables necessary for the *R*/*S* (Rescaled Range) analysis can be determined. Namely, the mean value of each subsequence $\mathcal{N}^{(j)}$ is computed as Mandelbrot and Wallis (1968, 1969); Mandelbrot (1982); Feder (1988):

$$\langle \mathcal{N}^{(j)} \rangle = \frac{1}{n} \sum_{i=1}^{n} N_{wc}(x_{j,i}), \tag{5}$$

where $\langle \mathcal{N}^{(j)} \rangle$ represents the average number of active wet channels within the j-th sequence. Next, the centered cumulative series is constructed as Mandelbrot and Wallis (1968, 1969); Mandelbrot (1982); Feder (1988):

$$Y^{(j)}(i) = \sum_{k=1}^{i} \left[N_{wc}(x_{j,k}) - \langle \mathcal{N}^{(j)} \rangle \right], \quad i = 1, \ldots, n, \tag{6}$$

which represents the cumulative deviation from the mean within each subsequence. The range $R^{(j)}(n)$ of the cumulative series is then defined as Mandelbrot and Wallis (1968, 1969); Mandelbrot (1982); Feder (1988):

$$R^{(j)}(n) = \max_{1 \le i \le n} Y^{(j)}(i) - \min_{1 \le i \le n} Y^{(j)}(i), \tag{7}$$

capturing the total spread of the centered cumulative process. The standard deviation of the original subsequence is calculated as Mandelbrot and Wallis (1968, 1969); Mandelbrot (1982); Feder (1988):

$$S^{(j)}(n) = \sqrt{\frac{1}{n} \sum_{i=1}^{n} \left[N_{wc}(x_{j,i}) - \langle \mathcal{N}^{(j)} \rangle \right]^2}, \tag{8}$$

which quantifies the local variability within the segment. Finally, the rescaled range statistic is obtained through the ratio Mandelbrot and Wallis (1968, 1969); Mandelbrot (1982); Feder (1988):

$$\left(\frac{R}{S} \right)_n^{(j)} = \frac{R^{(j)}(n)}{S^{(j)}(n)}, \tag{9}$$

which is the fundamental quantity used in the *R*/*S* analysis to assess the presence of long-range dependence. Note that subequences in Eq. (4) yielding zero standard deviation in N_{wc} were excluded from the rescaled-range computation, as the *R*/*S* statistic is undefined in these cases. Repeating the procedure for various values of n, the mean rescaled range over the k subsequences is calculated as Mandelbrot and Wallis (1968, 1969); Mandelbrot (1982); Feder (1988):

$$\mathbb{E}\left[R(n)/S(n) \right] = \frac{1}{k} \sum_{j=1}^{k} \left(\frac{R}{S} \right)_n^{(j)} \tag{10}$$

where $\mathbb{E}[\cdot]$ denotes the expected value (mean) over the k subsequences. The log-log analysis leads to the relationship Mandelbrot and Wallis (1968, 1969); Mandelbrot (1982); Feder (1988):

$$\mathbb{E}\left[R(n)/S(n) \right] \sim c \cdot n^H, \tag{11}$$

and therefore

$$\log\left(\mathbb{E}\left[R(n)/S(n) \right] \right) = \log c + H \cdot \log n. \tag{12}$$

The exponent H is estimated by linear least-squares regression in log–log space of $\log(R/S)$ versus $\log(n)$, selecting the fit over the range where the coefficient of determination R^2 is maximized $[n_{min}^{(r)}, n_{max}^{(r)}]$. In summary, the *R*/*S* analysis effectively characterizes the spatial structure of the number of active wet channels $N_{wc}(x)$ along the river. The Hurst exponent provides a quantitative measure of the braided river network's tendency toward persistence or anti-persistence. Specifically, the spatial interpretation of the Hurst exponent H reveals distinct behaviors: for $H < 0.5$, the system exhibits anti-persistent behavior, marked by frequent alternations between regions with few and many channels; for $H \approx 0.5$, the system lacks long-range dependence, though short-range correlations may still exist; and for $H > 0.5$, the system shows persistent behavior, where regions with a high density of channels tend to

be followed by other regions with similarly high density over larger spatial scales. Moreover, it is well established in the literature (Mandelbrot and Van Ness 1968; Mandelbrot 1985) that the Hurst exponent H is related to the fractal dimension D of a signal defined on a bidimensional support through the relation:

$$D = 2 - H. \tag{13}$$

where the factor 2 represents the dimension of the support. Eq. (13), commonly used for self-affine signals to estimate the fractal dimension of the signal support, assumes a different role within the framework of multifractal analysis. In this context, it is expressed in terms of the local singularity exponents α that define the multifractal spectrum and is directly related to the generalized Hurst exponents, as will be shown in the next section. Recently, Rizzello et al. (2024) related Eq. (13) to the TPL scale exponent using the relations by Kendal and Jørgensen (2011), yielding initial encouraging results when compared to multifractal measures obtained via a fixed-mass approach. These indirect results suggest a spatially persistent behavior of the number of wetted channels N_{wc} along their planimetric extent. Thus, the present work aims to extend and refine the findings of Rizzello et al. (2024) via a direct scaling approach, incorporating an initial explicit use of Eqs. (11) and (12) and, as discussed in the next section, a subsequent direct analysis based on Multifractal Detrended Fluctuation Analysis (MF-DFA).

2.3 Multifractal detrended fluctuation analysis (MF-DFA)

Multifractal Detrended Fluctuation Analysis (MF-DFA) was introduced by Kantelhardt et al. (2002) as a generalization of the standard Detrended Fluctuation Analysis (DFA) to detect multifractal scaling in nonstationary time series (Kantelhardt et al. 2001). It quantifies the generalized Hurst exponent $H(q)$, enabling the distinction between monofractal and multifractal behavior, even in the presence of trends. The method has been widely applied across disciplines such as statistical physics, econophysics, geophysics, and physiology due to its robustness against nonstationarities and its ability to disentangle multifractality arising from long-range correlations or broad distributions (Oświęcimka et al. 2006; Kantelhardt 2011). In the analysis of braided river systems, the MF-DFA methodology can be suitably extended to spatial signals N_{wc}, with the purpose of estimating the generalized Hurst exponent spectrum $H(q)$ and the associated multifractal spectrum $f(\alpha)$. This approach enables the characterization of spatial heterogeneity and reveals whether the signal N_{wc} exhibits persistent ($H(q) > 0.5$) or anti-persistent ($H(q) < 0.5$) behavior across scales in the morphological organization of braided systems. Therefore, given a one-dimensional discrete signal $N_{wc}(i)$ of length M, the mean value is computed as Kantelhardt et al. (2002):

$$\langle N_{wc} \rangle = \frac{1}{M} \sum_{i=1}^{M} N_{wc}(i) \tag{14}$$

and the centered cumulative profile is obtained through the following relation (Kantelhardt et al. 2001, 2002):

$$Y(i) = \sum_{k=1}^{i} \left(N_{wc}(k) - \langle N_{wc} \rangle \right). \tag{15}$$

Given the centered cumulative profile (Eq. (15)), the first step in the MF-DFA method consists in dividing the signal into $N_s = \lfloor \frac{M}{s} \rfloor$ non-overlapping segments of equal length s, where s is the scale parameter ranging within a predefined interval $[s_{\min}, s_{\max}]$. For each segment $\nu = 1, \ldots, N_s$, a polynomial fit of order m (typically $m = 1$ for linear detrending) is performed to remove local trends (Kantelhardt et al. 2001, 2002):

$$\begin{aligned} y_{\nu,\mathrm{fit}}(i) = &\text{polynomial of degree } m \\ &\text{fitted to } Y((\nu-1)s+i), \quad i = 1, \ldots, s. \end{aligned} \tag{16}$$

The detrended variance within each segment is then calculated as Kantelhardt et al. (2002):

$$F^2(\nu, s) = \frac{1}{s} \sum_{i=1}^{s} \left[Y((\nu-1)s+i) - y_{\nu,\mathrm{fit}}(i) \right]^2, \tag{17}$$

and so, for $\nu = N_s + 1, \ldots, 2N_s$ the equation (17) becomes (Kantelhardt et al. 2002):

$$F^2(\nu, s) = \frac{1}{s} \sum_{i=1}^{s} \left[Y(N - (\nu - N_s)s + i) - y_{\nu,\mathrm{fit}}(i) \right]^2. \tag{18}$$

The q-order fluctuation function is defined for $q \neq 0$ as Kantelhardt et al. (2002):

$$F_q(s) = \left\{ \frac{1}{N_s} \sum_{\nu=1}^{N_s} \left[F^2(\nu, s) \right]^{q/2} \right\}^{1/q}, \tag{19}$$

and, for $q = 0$, using a logarithmic average (Kantelhardt et al. 2002):

$$F_0(s) = \exp\left\{ \frac{1}{2N_s} \sum_{\nu=1}^{N_s} \ln \left[F^2(\nu, s) \right] \right\}. \tag{20}$$

By repeating the computation for multiple scales s, a power-law relation is expected (Kantelhardt et al. 2002):

$$F_q(s) \sim s^{H(q)}, \tag{21}$$

where the generalized Hurst exponent $H(q)$ is estimated via a linear fit in log-log coordinates (Kantelhardt et al. 2002):

$$\log F_q(s) = H(q) \log s + C(q), \tag{22}$$

with $C(q)$ a constant, and where the coefficient of determination R^2 is maximum.

From the generalized Hurst exponent spectrum $H(q)$, one can derive the sequence of mass exponents $\tau(q)$ and, through a Legendre transform, the singularity spectrum $f(\alpha)$, which provides a geometrical description of the multifractality in the signal (N_{wc}). The sequence of mass exponents is defined as Kantelhardt et al. (2002):

$$\tau(q) = qH(q) - 1, \tag{23}$$

while the singularity strength $\alpha(q)$, also referred to as the Hölder exponent, is given by the first derivative of $\tau(q)$ with respect to q (Kantelhardt et al. 2002):

$$\alpha(q) = \frac{d\tau(q)}{dq} = \frac{d}{dq}\big(qH(q) - 1\big). \tag{24}$$

The multifractal spectrum $f(\alpha)$ is then obtained via the Legendre transform (Kantelhardt et al. 2002):

$$f(\alpha) = q\alpha - \tau(q) = q\alpha - \big(qH(q) - 1\big). \tag{25}$$

The function $f(\alpha)$ characterizes the distribution of singularities in the signal and their corresponding fractal dimensions. The width of the multifractal spectrum $f(\alpha)$ reflects the range of scaling exponents present in the signal (N_{wc}), with a wider spectrum indicating stronger multifractality and greater complexity in the local fluctuations, reflecting a richer variability of local scaling exponents. The position of the maximum of $f(\alpha)$, typically corresponding to the most probable singularity exponent, provides insight into the dominant scaling behavior and can be related to the overall roughness or regularity of the signal (N_{wc}). In summary, the multifractal spectrum, defined by the function $f(\alpha)$, provides a detailed description of the distribution of local singularities α, which correspond to the pointwise Hölder exponents of the signal N_{wc}. The value α_0, at which $f(\alpha)$ attains its maximum, represents the dominant singularity, namely the most frequent regularity in the spatial signal N_{wc}. These aspects are well known in the literature and provide useful guidance for a reliable estimation of the scaling exponents characterizing the scaling process of the spatial signal N_{wc}. Therefore, according to Mandelbrot (1986), Badii and Politi (1984, 1985), Bacry et al. (1993), Muzy et al. (1993) and Pesin (1997), the fractal dimension, D, of the signal N_{wc} can be considered as the local mass dimension or pointwise dimension, which is equal to the Hölder exponent α in Eq. (24). Hence, an accurate estimation of the singularity exponents α, and in particular of the maximum one α_0, constitutes a fundamental scaling parameter to be estimated and compared with the generalized exponents $H(q)$, namely when $H(0) \approx \alpha_0$. From a theoretical point of view, this approximation can be straightforwardly verified through simple analytical steps. By differentiating Eq. (23) with respect to q, one obtains in general that Eq. (24) becomes

$$\alpha(q) = \frac{d\tau(q)}{dq} = H(q) + q\frac{dH(q)}{dq}, \tag{26}$$

and, therefore, for $q = 0$, it follows that $H(0) = \alpha(0)$. Thus, any minor differences between $H(0)$ and $\alpha(0)$ are solely due to the numerical derivatives involved in the Legendre transform and in the relation (24).

3 Data analysis and results

3.1 Brahmaputra braided river data

The spatial persistence in braided river networks, based on equations (11)–(12) and (21)–(25), was investigated exclusively on the spatial configurations of the Braided Channel Networks (BCNs) of the Brahmaputra River, considering their temporal evolution across 12 different configurations obtained from satellite images acquired between 1976 and 2007 at varying time intervals. The satellite imagery was sourced from Landsat MSS, Landsat TM, IRS LISS, and ASTER. All these fluvial systems exhibit geomorphological features and spatiotemporal variability characteristic of braided river environments. As example, Fig. 1 shows the Brahmaputra River derived from 1987 satellite imagery, with the indication of initial (left) and final (right) transects used to estimate the number of active channels. The datasets employed in this study were previously compiled and documented in Rizzello et al. (2023, 2024). For comprehensive technical details regarding data acquisition and preprocessing methods, the reader is referred to these references. As previously mentioned, the Brahmaputra River is a trans-boundary, large, sand-bed, mildly sloping braided river that flows from the Eastern Himalayas across the Bengal Basin to the Ganges-Brahmaputra-Meghna delta in the Bay of Bengal. For further specialized reading on the fluvial

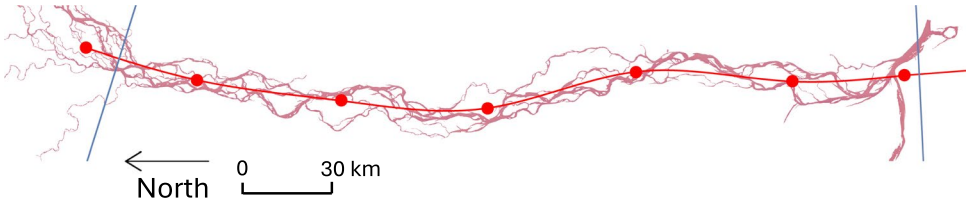

Fig. 1 The Brahmaputra River as derived from 1987 satellite imagery, showing the initial (left) and final (right) transects (in blue) used to estimate the number of active channels, at a spatial resolution of 80 m. The red line with dots indicates the curvilinear abscissa along the river. The coordinates of the first (leftmost) and last red dots are (25° 46'56.52"N, 89°52'31.29"E) and (23°45'23.98"N, 89°47'26.60"E), respectively

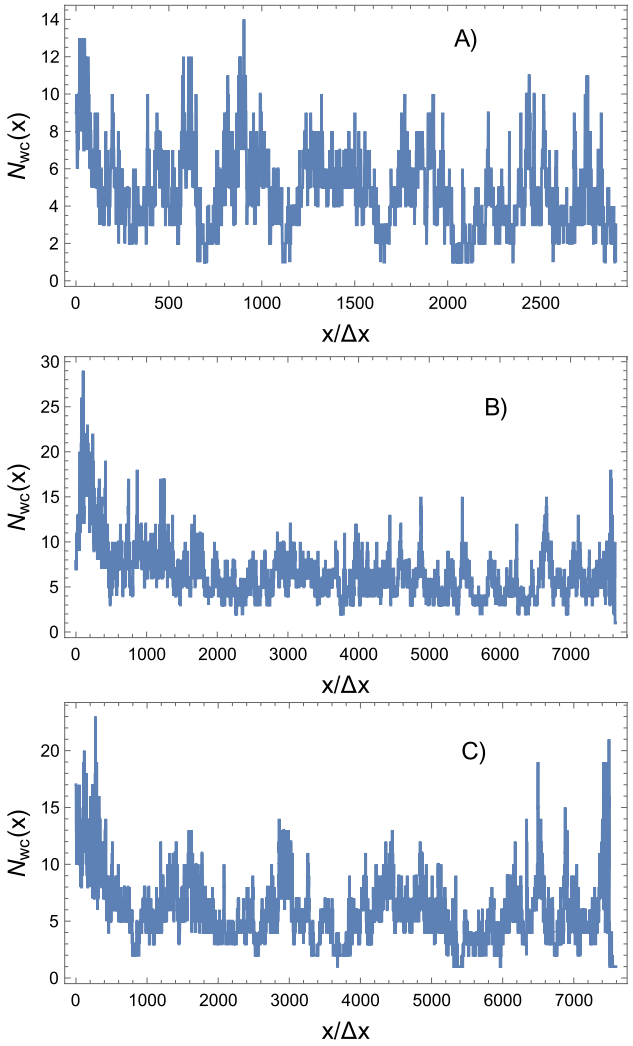

Fig. 2 Examples of the variation of the number of wet channels, N_{wc}, as a function of $x/\Delta x$ (progressive number of transects) for three different years. A) N_{wc} in 1976, derived from the Landsat MSS acquisition of 10 January 1976 with a spatial resolution of 80 × 80 m. B) N_{wc} in 1989, derived from the Landsat TM acquisition of 28 February 1989 with a spatial resolution of 30 × 30 m. C) N_{wc} in 1999, derived from the Landsat TM acquisition of 23 January 1999 with a spatial resolution of 30 × 30 m

Table 1 Satellite imagery and spatial resolutions used in the analysis of the Brahmaputra River

Satellite	Resolution (m^2)	Time period	Acquisitions
Landsat MSS	80 × 80	10 Jan 1976–7 Feb 1987	6
Landsat TM	30 × 30	28 Feb 1989–23 Jan 1999	4
IRS LISS	24 × 24	5 Feb 2005	1
ASTER	15 × 15	14 Jan 2007	1

geomorphology of the Brahmaputra River—particularly regarding braided dynamics, channel evolution, and modeling approaches - the reader is referred to Sarma (2005); SahDas 2018; Gogoi (2018); Singh (2004); Lahiri (2023), which offer comprehensive overviews and case-specific insights.

The spatial resolutions considered were as follows: 80 m × 80 m for the period from 10 January 1976 to 7 February 1987 using Landsat MSS imagery (6 acquisitions); 30 m × 30 m for the period from 28 February 1989 to 23 January 1999 using Landsat TM imagery (5 acquisitions); 24 m × 24 m for 5 February 2005 using IRS LISS imagery (single acquisition); and finally, 15 m × 15 m for 14 January 2007 using ASTER imagery (single acquisition). A detailed summary of the spatial resolutions and temporal coverage of the satellite imagery is provided in Table 1.

For each satellite image, with spatial resolution $\Delta x = 15, 24, 30$, and 80 m, and for each year considered, we extracted the total number of elements M of the discrete series $\mathcal{N}$ defined in Eq. (3), consisting of integer values $N_{wc}(x_i)$. Each series (12 in total) is characterized by equally spaced positions x_i, determined by the resolution Δx. Consequently, 15, 24, 30, and 80 m represent the minimum spacing between consecutive transects used to count the number of wetted (active) channels. Accordingly, the following were obtained: for $\Delta x = 15$ m, a series with $M = 14515$, corresponding to a longitudinal planimetric extent of about 218 km; for $\Delta x = 24$ m, a series with $M = 9614$, corresponding to about 231 km; for $\Delta x = 30$ m, five series were extracted, with a minimum of $M = 7574$ and a maximum of $M = 9614$ elements, characterized by an average of $M = 8053.11$ elements and a mean longitudinal

extent of about 242 km; and for $\Delta x = 80$ m, six series were extracted, with a minimum of $M = 2905$ and a maximum of $M = 7637$ elements, characterized by an average of $M = 4441.5$ elements and a mean longitudinal extent of about 355 km. In order to illustrate the temporal evolution of the number of wet channels, Fig. 2 reports three representative examples of N_{wc} as a function of the abscissa x for different years. Panel A) refers to the year 1976, where N_{wc} was obtained from the Landsat MSS scene acquired on 10 January 1976, characterized by a spatial resolution of 80×80 m. Panel B) corresponds to the year 1989, and shows N_{wc} derived from the Landsat TM acquisition of 28 February 1989, with a finer spatial resolution of 30×30 m. Finally, Panel C) presents the case of the year 1999, based on the Landsat TM scene acquired on 23 January 1999, also with a resolution of 30×30 m. These three examples provide a direct comparison of the behavior of wet channels across different time periods and acquisition conditions.

3.2 Rescaled range (*R*/*S*) analysis of the Brahmaputra braided river

The Hurst exponents H were obtained from Eqs. (11–12), while the fractal dimensions D were derived from Eq. (13). The estimation procedure was implemented in Mathematica, ensuring an efficient handling of the window lengths n over which the rescaled range R/S was computed according to Eqs. (7), (8), and (10). The procedure optimizes the selection of the scaling interval $[n_{min}^{(r)}, n_{max}^{(r)}]$ where the coefficient of determination R^2 is maximized. Accordingly, the analysis allowed us to identify the lower and upper cut-off limits as a function of the total signal length $M(N_{wc})$, within an interval starting from $n_{min} = 4$ up to $n_{max} \approx M/4$. In terms of the characteristic lengths of the R/S scaling, these values depend on the satellite image spatial resolution Δx and range approximately from $4 \cdot \Delta x$ to $M/4 \cdot \Delta x$. The choice of the maximum limit $M/4$ for the largest window ensures that there are enough segments even at the largest scales, and, as we will see shortly, this choice is motivated by the search for the maximum coefficient of determination R^2. In addition, this phase of the analysis considered the effect of the window step size, Δn, which denotes the window length n, in the direct scaling. Specifically, the selection of the optimal scaling range is based on the criterion of maximizing the coefficient of determination R^2, for each of the 12 datasets we determined not only the cut-off limits n_{min} and n_{max}, but also the maximum admissible step size (Δn). Figure 3A–D illustrate, as examples, selected scalings obtained from Eq. (12), i.e., plots of $\mathbb{E}[R(n)/S(n)]$ versus $\log n$.

Figure 3a shows the $\mathbb{E}[R(n)/S(n)]$ scaling versus n for the Brahmaputra Braided River, derived from the 1976 Landsat image at 80×80 m spatial resolution. The analysis uses $n_{min}^{(r)} = 10$ (800 m) and $n_{max}^{(r)} = 726$ (58 km) from a total length $M = 2905$. The estimated Hurst exponent is 0.946 with $R^2 = 0.993$, while the fractal dimension $D = 1.05$. Figure 3b–d illustrate how the $\mathbb{E}[R(n)/S(n)]$ scaling versus n depends also on the step size (Δn) values, with all three figures referring to the Brahmaputra Braided River derived from the 2007 ASTER image, and with $n_{min} = 4$, $n_{max} = 3628$ and $M = 14515$, corresponding to approximately 54 km. Specifically, Fig.3b, c, d illustrate how the estimates of H and D depend on the step size, with Δn = 4, 50, 150, respectively, with $n_{min}^{(r)} = n_{min}$ and $n_{max}^{(r)} = n_{max}$. The three cases yielded Hurst exponents of 0.969, 0.962, and 0.975, with $R^2 = 0.997$, 0.997, and 0.996, respectively. The analysis procedure was applied to all remaining datasets, indicating that the Hurst exponent and fractal dimension are optimally estimated with $n_{min}^{(r)} = 10$, $n_{max}^{(r)} \approx M/4$, and step size Δn = 10, where the coefficient of determination R^2 reached its maximum, corresponding to the highest goodness-of-fit for the model. Table 2 reports all numerical results for the 12 datasets under these settings.

It is worth noting that, in all cases analyzed, the Hurst exponent H exceeded $\frac{1}{2}$, revealing a generally persistent behavior of the spatial signal N_{wc}. In addition, we have calculated, for each year of the dataset, the autocorrelation function and the spectral density function (not reported here for brevity). The results showed the persistence of the autocorrelation at large lags and a power law behavior of the spectral density function with Hurst exponent values $H > 0.5$ indicating persistent spatial behavior in the braiding index signal. Persistent behavior indicates long-range spatial organization of the channel network, whereby reaches with a large number of active channels tend to occur within extended portions of the river that also exhibit high channel density. This pattern reflects a degree of morphological coherence in the braided system, associated with relatively uniform flow conditions, sediment supply, and channel-forming processes, as well as strong lateral connectivity within the Brahmaputra fluvial system. The results are in fair agreement with those of De Bartolo et al. (2022) and Rizzello et al. (2024) on other braided river systems analyzed through the generalized TPL law. The observed difference between the maximum ($H = 0.999$) and minimum ($H = 0.897$) Hurst exponents, about 10%, points to a degree of scale invariance of both the exponent and the associated fractal dimension across changes in spatial resolution. Still, because the R/S method assumes simple (monofractal) scaling, it tends to overestimate H when compared with generalized local techniques such as MF-DFA, as already noted by Rizzello et al. (2024) De Michele et al. (2025) and further discussed in the next section in terms of multifractal

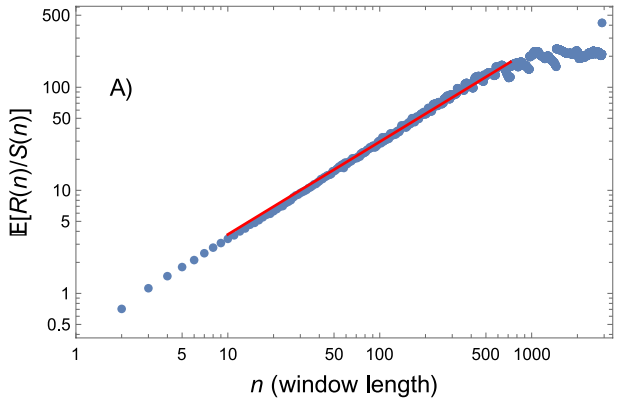

(A) $\mathbb{E}\,[R(n)/S(n)]$ versus n in the range $[2, 2905]$ with step size $\Delta n = 1$, and $n_{min}^{(r)} = 10$, $n_{max}^{(r)} = 726$, derived from the 1976 Landsat MSS image.

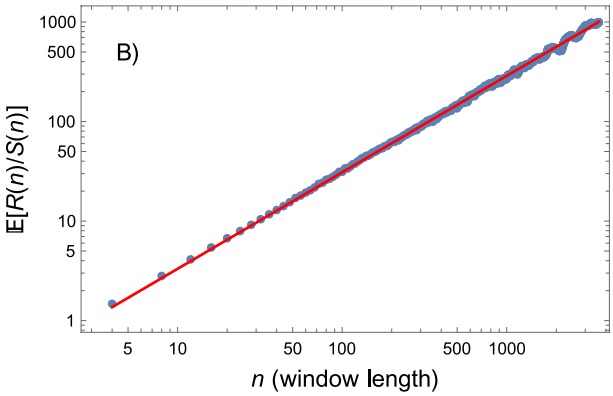

(B) $\mathbb{E}\,[R(n)/S(n)]$ versus n, with $n_{min} = 4$, $n_{max} = 3628$, and step size $\Delta n = 4$, derived from the 2007 ASTER image.

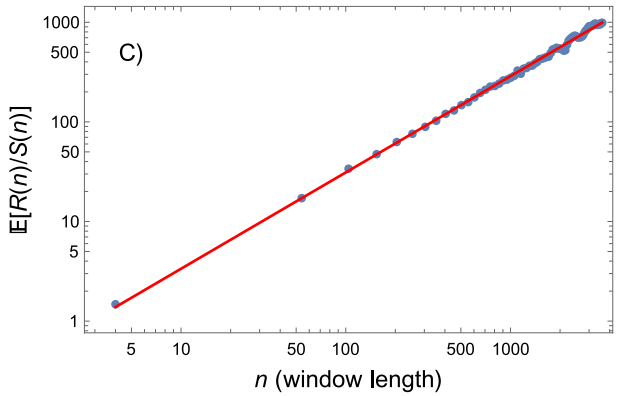

(C) $\mathbb{E}\,[R(n)/S(n)]$ versus n, with $n_{min} = 4$, $n_{max} = 3628$, and step size $\Delta n = 50$, derived from the 2007 ASTER image.

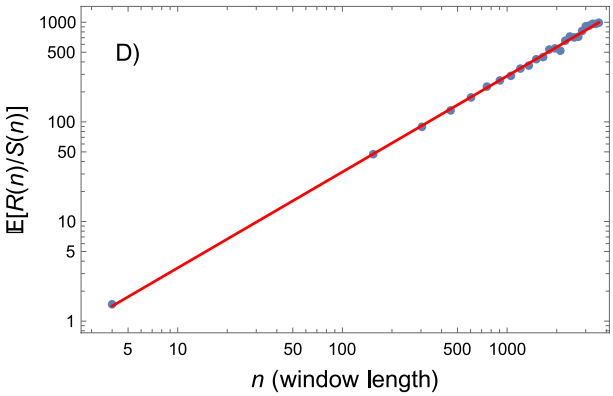

(D) $\mathbb{E}\,[R(n)/S(n)]$ versus n, with $n_{min} = 4$, $n_{max} = 3628$, and step size $\Delta n = 150$, derived from the 2007 ASTER image.

Fig. 3 R/S analysis of the Brahmaputra River: parameter characterization of the scaling given by Eq. (12)

Table 2 Rescaled Range (*R*/*S*) Analysis of the Brahmaputra braided river. The first column reports the year of acquisition of the satellite image. H denotes the estimated Hurst exponent, D is the fractal dimension obtained from the relation $D = 2 - H$ (Eq. 13), and R^2 represents the coefficient of determination of the regression used to estimate H

Year	H	D	R^2
1976	0.946	1.05	0.993
1977	0.925	1.07	0.997
1978	0.956	1.04	0.996
1980	0.915	1.08	0.991
1985	0.899	1.10	0.995
1987	0.897	1.10	0.997
1989	0.992	1.01	0.996
1992	0.997	1.07	0.996
1997	0.972	1.03	0.996
1999	0.940	1.06	0.995
2005	0.999	1.00	0.995
2007	0.969	1.03	0.997

measures. Nevertheless, the monofractal *R*/*S* scaling results can offer useful preliminary guidance for choosing the scale parameters s_{min}, s_{max}, and step size (Δs) in MF-DFA analyses, aimed at estimating generalized Hurst exponents $H(q)$ and multifractal spectra $f(\alpha)$, including the associated local singularity exponents α. Along with these parameters, the *R*/*S* analysis with $H > \frac{1}{2}$ suggests, through the spatial persistence of the N_{wc} signal, a potential correlation with the discharge Q that drives the braided morphology of the analyzed river systems. Although simultaneous time series are not available, referring to the discharge estimates for the Brahmaputra River in different years reported by Rizzello et al. (2024) - i.e., a non-equally spaced chronology - the *R*/*S* analysis, as shown in Fig. 4, indicates a substantial invariance of H with discharge, with values close to unity.

Specifically, Fig. 4 shows $\langle N_{wc} \rangle$ with the standard deviation (vertical bars) and the Hurst exponent, H, as functions

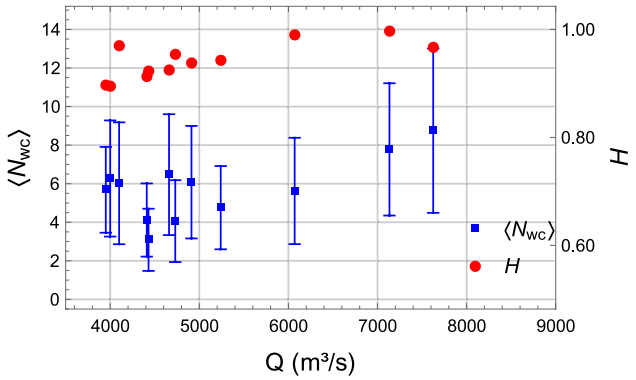

Fig. 4 Variation of $\langle N_{wc} \rangle$ with the standard deviation (vertical bars) and the Hurst exponent, H, as a function of the discharge Q (m^3/s) for the Brahmaputra River. The data are shown in increasing order from 1976 to 2007

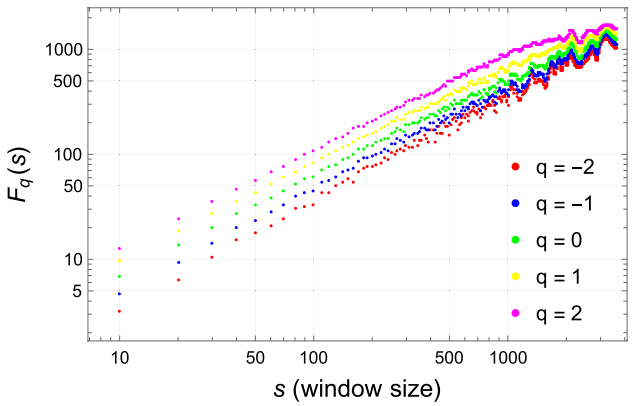

Fig. 5 Example of the scaling behavior of $F_q(s)$ vs s. The reference dataset is the 2007 ASTER image

of the discharge Q (m^3/s), presented in increasing order from 1967 to 2007. Extending this investigation to additional time series with equally spaced chronological sampling will be crucial to determine whether the observed persistence is strongly influenced by the discharge and to identify potential critical threshold values, thus providing a deeper understanding of the dynamics governing braided river systems. These observations align with experimental and theoretical studies, which consistently show that braided river morphology becomes more complex and exhibits stabilized spatial persistence of active channels with increasing discharge or stream power (e.g., Egozi and Ashmore 2009; Bertoldi et al. 2009; see also Ashmore 2009, for a general review on braiding intensity and discharge relationships).

In conclusion, the *R*/*S* analysis provides a fast, first-order estimate of the degree of persistence in the N_{wc} signal across the analyzed river reaches, offering a direct quantitative descriptor of large-scale spatial organization in braided systems in terms of simple (non-fractal) scaling. While we recognize that rescaled-range analysis may be influenced by non-stationarity and short-range dependence, in this study it is used as an exploratory tool to characterize system-scale spatial coherence rather than as definitive evidence of a stationary long-memory process. This analysis therefore serves as a preliminary step to be complemented by multiscaling approaches. In the following section, we extend this framework using multifractal MF-DFA analysis to estimate the multifractal spectrum $f(\alpha)$ and the local singularity exponents α, which provide a more detailed and scale-resolved characterization of the spatial organization and persistence of the N_{wc} signals.

3.3 Multifractal detrended fluctuation analysis (MF-DFA) of the Brahmaputra braided river

The preliminary *R*/*S* analysis previously carried out provided precise indications on the spatial window range to be considered, namely $n \in [n_{min}, n_{max}]$, for determining the persistence scaling of the signal N_{wc}. In accordance with the formalism introduced in Sect. 2.3, this interval will now take the symbolic form $s \in [s_{min}, s_{max}]$, with step size Δs. Consequently, the vector of observation scales, i.e., the set of window lengths in which the signal is partitioned to estimate how the fluctuations of N_{wc} vary with scale in the MF-DFA method, will be represented by the set $\{s_{min},\ s_{min} + \Delta s,\ s_{min} + 2 \cdot \Delta s,\ \ldots,\ s_{max}\}$. A preliminary analysis also allowed us to define, through the maximization of the coefficient of determination R^2, the optimal window interval for estimating the scaling of $F_q(s)$ versus s as given by Eqs. 21 and 22, namely $s_{min} = 10$ and $s_{max} = M/4$, with $\Delta s = 10$. As in the *R*/*S* analysis, the choice of the largest window s_{max}, equal to one-fourth of the total signal length, ensures that a sufficient number of segments $N_s = \lfloor \frac{M}{s} \rfloor$ is available even for the largest scales. Summarizing, the procedure performed for each s in the observation scale vector consisted of the following steps: the signal is divided into segments of length s; the local variance $F^2(\nu, s)$ on each segment is computed using Eq. 17; the resulting values are combined to obtain the functions in Eqs. 19 and 20; the process is repeated for various $s \in [s_{min}, s_{max}]$ to construct the $F_q(s)$ versus s curve. This procedure was carried out for all 12 satellite data sets considered in this study.

In agreement with Rizzello et al. (2024) and De Michele et al. (2025), given the large number of signals N_{wc} considered, the range of investigation for the moment order q was set to the interval $[-5, 5]$, with an increment of $\Delta q = 0.5$, in order to reduce estimation errors in the Legendre transform of the multifractal spectra, particularly for the singularities α_0, α_{max}, and α_{min}. Particular attention was devoted to the singularity at $q = 0$, as expressed by Eq. 20, since the value $H(0)$ requires careful treatment. Indeed, the function $F_q(s)$

is not defined in the direct limit at $q = 0$, and unrealistically high values of $H(0)$ are often observed, which may indicate the presence of low-variance segments or numerical ill-conditioning. Therefore, following (Kantelhardt et al. 2002), a logarithmic averaging approach was adopted to ensure the consistency of Eq. 20. Finally, using Eqs. 21 and 22, the scalings of $F_q(s)$ versus s were directly estimated. These allowed us to first derive the generalized spectrum of Hurst exponents $H(q)$, and subsequently, through the sequence of mass exponents $\tau(q)$ (Eq. 23) and the Legendre transform (see Eqs. 24 and 25), to obtain the multifractal spectrum $f(\alpha)$ together with the local singularities α. Figure 5 shows an example of the MF-DFA scaling, $F_q(s)$ versus s, computed for the 2007 ASTER image. The plot illustrates the scaling behavior for some values of q in the estimation range $[-5, 5]$.

In Fig. 6a-d, as an example, only a selection of the estimated generalized spectra $H(q)$ and $f(\alpha)$ is shown, corresponding to the analysis conducted on the considered braided systems.

Specifically, Fig. 6a shows the generalized Hurst exponents $H(q)$ for the Brahmaputra Braided River, derived from the 1976 Landsat MSS image, with $s_{min} = 10$, $s_{max} = 726$, and step size $\Delta s = 10$, while Fig. 6b displays the corresponding multifractal spectrum $f(\alpha)$ for the same river and image, with the same parameters. Similarly, Fig. 6cpresents the generalized Hurst exponents $H(q)$ for the Brahmaputra Braided River, derived from the 1999 Landsat TM image, with $s_{min} = 10$, $s_{max} = 1903$, and step size $\Delta s = 10$, and Fig. 6d shows the corresponding multifractal spectrum $f(\alpha)$ for this latter image, with the same parameters. Table 3 summarizes, for all 12 analyzed cases, the numerical values of the most significant parameters of the Multifractal Detrended Fluctuation Analysis (MF-DFA) of the Brahmaputra Braided River. Specifically, Table 3 reports the reference year of the satellite image, the Hurst exponent $H(0)$ evaluated at $q = 0$, the singularity α_0 corresponding to $q = 0$, the absolute difference between these two quantities, the minimum (α_{min}) and maximum (α_{max}) values of the estimated singularities α, and the difference $\Delta\alpha = \alpha_{max} - \alpha_{min}$, which quantifies the width of the multifractal spectrum $f(\alpha)$.

The results first indicate that, through the Multifractal Detrended Fluctuation Analysis (MF-DFA), the local Hurst exponents $H(0)$, i.e., those evaluated at $q = 0$, are lower than those estimated through the global R/S scaling previously discussed, with the exception of the year 1987; however, this represents a single observed case. These values, as anticipated already in Sect. 2.1, were entirely expected, since the R/S analysis offers a straightforward estimation of long-range dependence under monofractal assumptions, whereas MF-DFA extends the analysis to capture scale-dependent fluctuations and heterogeneity in the scaling behavior, making it particularly suitable for detecting multifractal features in complex spatial signals such as N_{wc}. Overall, these results are fully consistent with those preliminarily evaluated, including on different datasets, by Rizzello et al. (2024) using the generalized TPL procedure, as well as with those recently reported by De Michele et al. (2025) in the context of a multiscaling analysis conducted through the structure functions $S_q(l)$. Indeed, these latter authors, as anticipated in the Sect. 2.1, have clearly highlighted that, for braided river systems, and in particular for the Brahmaputra River, the direct estimation of multifractal spectra tends to be underestimated when using structure functions, compared to the usual direct multifractal techniques based on fixed size and fixed mass. Consequently, the associated scaling parameters, such as the exponent function $\zeta(q)$ and the Hurst exponent itself, are also underestimated. De Michele et al. (2025) addressed this discrepancy, which had already been pointed out by Bacry et al. (1993), Muzy et al. (1993), by introducing corrective factors on the scaling function $\zeta(q)$, and consequently also on the multifractal spectra derived from the Legendre transform. Therefore, in agreement with what was anticipated in Sect. 2.3, the Multifractal Detrended Fluctuation Analysis (MF-DFA) procedure bypasses these uncertainties, as it provides a direct comparison with the singularity α_0, which represents the dominant singularity, namely the most frequent regularity in the spatial signal N_{wc}.

Another important aspect highlighted by the MF-DFA is that the estimated values of $H(0)$, ranging between 0.764 (minimum) and 0.943 (maximum), consistently confirmed the persistent behavior of all the spatial signals N_{wc} considered. Moreover, the relative differences $|H(0) - \alpha_0|$ showed a substantial agreement between the estimated values of $H(0)$ and α_0, indicating a good reliability of the MF-DFA procedure ($H(0) \approx \alpha_0$). This is in line with previous studies by Mandelbrot (1986), Badii and Politi (1984), Badii and Politi (1985), Bacry et al. (1993), Muzy et al. (1993), Pesin (1997), which report that, for the fractal dimension D of the signal N_{wc}, the local (or pointwise) mass dimensions are equal to the Hölder exponent α in Eq. (24). The results also show clear signs of persistence for all the signals considered, as evidenced by the minimum generalized Hurst exponents $H(q)$ evaluated at $q = 5$. Indeed, according to Eq. (24), the generalized function $H(q)$ has the same form as $\alpha(q)$, although shifted upward, but with $H(0) \approx \alpha_0$. Consequently, the minimum values of $H(q)$ were all greater than $\frac{1}{2}$, ranging between 0.565 and 0.682. Therefore, similar to the R/S analysis, the MF-DFA highlights a potential persistent behavior of the number of active wet channels N_{wc} in relation to the flow, and in particular as discharge increases. Consistent with the results shown for the R/S analysis, and

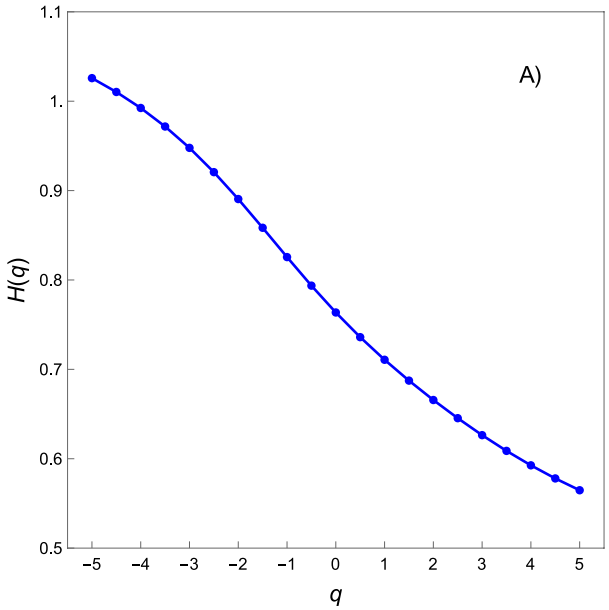

(A) Generalized Hurst exponents $H(q)$ for the Brahmaputra Braided River, derived from the 1976 Landsat MSS image, with $s_{min} = 10$, $s_{max} = 726$, and step size $\Delta s = 10$.

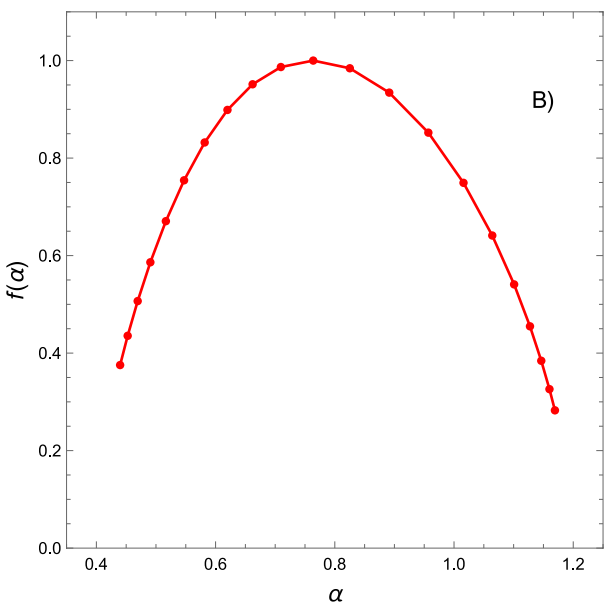

(B) Multifractal spectrum $f(\alpha)$ for the Brahmaputra Braided River, derived from the 1976 Landsat MSS image, with $s_{min} = 10$, $s_{max} = 726$, and step size $\Delta s = 10$.

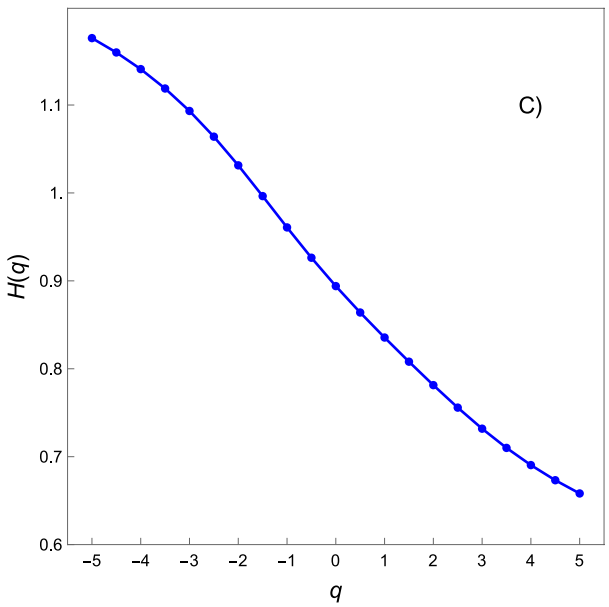

(C) Generalized Hurst exponents $H(q)$ for the Brahmaputra Braided River, derived from the 1999 Landsat TM image, with $s_{min} = 10$, $s_{max} = 1903$, and step size $\Delta s = 10$.

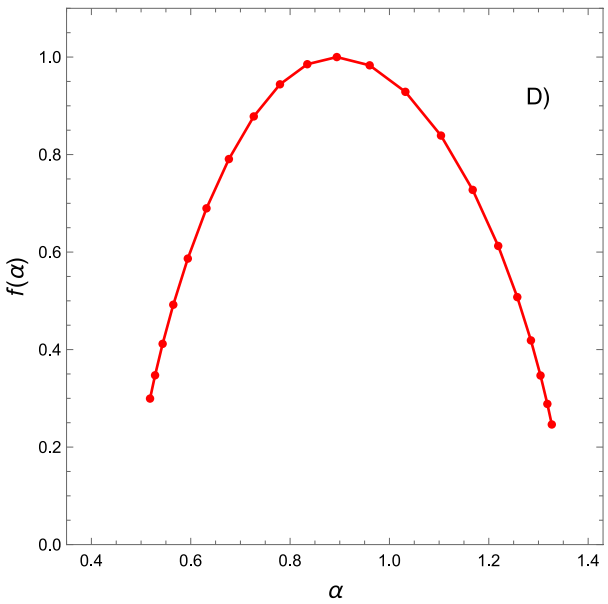

(D) Multifractal spectrum $f(\alpha)$ for the Brahmaputra Braided River, derived from the 1999 Landsat TM image, with $s_{min} = 10$, $s_{max} = 1903$, and step size $\Delta s = 10$.

Fig. 6 Multifractal detrended fluctuation analysis (MF-DFA) of the Brahmaputra braided river: generalized Hurst exponents $H(q)$ and multifractal spectra $f(\alpha)$

based on the main parameters estimated through the MF-DFA, it is possible to observe (not shown for brevity), a substantial invariance of the exponents $H(0)$ and α_0 with the discharge. This finding is in agreement with the previously stated conclusion that these observations align with experimental and theoretical studies, which consistently show that braided river morphology becomes more complex and exhibits stabilized spatial persistence of active channels with

Table 3 Multifractal detrended fluctuation analysis (MF-DFA) of the Brahmaputra braided river

Year	$H(0)$	α_0	$\lvert H(0)-\alpha_0\rvert$	α_{min}	α_{max}	Δ_α
1976	0.764	0.764	0.0001	0.439	1.169	0.730
1977	0.884	0.884	0.0002	0.505	1.257	0.752
1978	0.801	0.801	0.0004	0.592	1.310	0.718
1980	0.887	0.886	0.001	0.565	1.310	0.792
1985	0.764	0.764	0.0003	0.557	0.983	0.426
1987	0.943	0.943	0.0007	0.505	1.283	0.778
1989	0.875	0.875	0.0004	0.456	1.263	0.807
1992	0.848	0.848	0.0001	0.491	1.162	0.671
1997	0.889	0.888	0.001	0.520	1.309	0.789
1999	0.894	0.894	0.000002	0.518	1.326	0.808
2005	0.883	0.883	0.0002	0.448	1.249	0.801
2007	0.868	0.868	0.00015	0.464	1.187	0.723

The first column reports the year of acquisition of the satellite image. $H(0)$ denotes the generalized Hurst exponent for $q = 0$. α_0 is the position of the maximum of the multifractal spectrum, and $|H(0) - \alpha_0|$ measures the deviation between the two scaling exponents. α_{min} and α_{max} are the minimum and maximum values of the singularity strength, respectively, while $\Delta\alpha = \alpha_{max} - \alpha_{min}$ quantifies the width of the multifractal spectrum

increasing discharge or stream power (Egozi and Ashmore 2009; Bertoldi et al. 2009; Ashmore 2009). It is also important to emphasize that, based on the estimation of the $f(\alpha)$ spectra, another significant parameter that emerged from this MF-DFA analysis is the relatively uniform distribution of the multifractal spectrum widths, $\Delta\alpha$, with a meaningful average value of 0.738. These results are very close to those recently obtained by De Michele et al. (2025) using fixed-mass direct multifractal procedures. These findings suggest that, despite temporal and spatial variations in channel configuration and discharges, the multifractal complexity of the active channel network N_{wc} remains essentially stable. The similar amplitudes of the multifractal spectra, $\Delta\alpha$, across all 12 spatial series indicate that the braided river system is governed by intrinsic self-organizing processes, maintaining a consistent hierarchy of spatial structures over time. This reflects a stable multifractal signature of the river morphology, where local changes in channel positions and numbers do not alter the overall scaling heterogeneity of the system, in agreement with previous studies on braided river dynamics (Egozi and Ashmore 2009; Bertoldi et al. 2009; Ashmore 2009).

4 Conclusions

The present study aimed to enhance the robustness in estimating the Hurst exponent for complex spatial signals of braided rivers by applying two complementary methodologies: the classical Rescaled Range (R/S) Analysis and the Multifractal Detrended Fluctuation Analysis (MF-DFA). While the R/S analysis provided a direct estimation of long-range dependence under monofractal assumptions, the MF-DFA allowed for a deeper characterization of scale-dependent fluctuations and heterogeneity in the scaling behavior, enabling the detection of multifractal features in the spatial signal representing the number of active channels, N_{wc}.

The analysis was carried out on 12 spatial datasets of the Brahmaputra braided river system, derived from multisource satellite imagery spanning over three decades with varying spatial resolutions. The R/S results consistently indicated persistence across all examined signals ($H > \frac{1}{2}$), implying positive spatial correlations. This suggests that river sections with a high number of active channels tend to occur within extended portions of the river that also exhibit elevated channel density, reflecting a coherent morphological organization associated with relatively uniform flow conditions, sediment supply, and strong lateral connectivity.

The MF-DFA confirmed these findings and provided additional insights by capturing the multifractal nature of the system. The estimated local Hurst exponents, $H(0)$, were consistently lower than those obtained through the global R/S scaling, highlighting the ability of MF-DFA to account for local variations and heterogeneities. Moreover, the similarity of the multifractal spectrum widths, $\Delta\alpha$, across all 12 datasets indicates a stable multifractal signature of the braided river morphology. This finding suggests that, despite temporal variations in channel configuration and discharge, the underlying complexity and hierarchical organization of the system remain essentially invariant over time, consistent with the presence of intrinsic self-organizing processes.

From a geomorphological and hydraulic perspective, these results imply that the persistence observed in N_{wc} reflects a stable network structure where local changes in channel positions or numbers do not alter the overall scaling heterogeneity. This supports the view that braided rivers,

such as the Brahmaputra, at least for the cases analyzed, maintain a balance between channel migration, bifurcation, and sediment dynamics, leading to a characteristic and stable multifractal pattern.

In conclusion, combining *R*/*S* analysis and MF-DFA proved to be an effective strategy for characterizing the spatial organization of braided river systems. Future work should aim to extend this approach to other river systems with different morphological and hydrological conditions, as well as to integrate temporal analyses, which would further improve our understanding of the dynamic processes shaping these complex fluvial environments.

Acknowledgements

C.D.M. was supported by the RETURN project (Multi-risk science for resilient commu-611nities under a changing climate) with Extended Partnership, which received funding from612the European Union Next-GenerationEU, National Recovery and Resilience Plan—NRRP,613Mission 4, Component 2, Investment 1.3—D.D. 1243 2/8/2022, PE0000005.

Acknowledgments C.D.M. was supported by the RETURN project (Multi-risk science for resilient commu-611nities under a changing climate) with Extended Partnership, which received funding from612the European Union Next-GenerationEU, National Recovery and Resilience Plan—NRRP,613Mission 4, Component 2, Investment 1.3—D.D. 1243 2/8/2022, PE0000005.

Author contributions Samuele De Bartolo: Writing—review and editing, Writing—original draft, Visualization, Validation, Supervision, Software, Methodology, Investigation, Formal analysis, Data curation, Conceptualization. Carlo De Michele: Writing, Methodology, Investigation, Formal analysis, Data curation, Conceptualization. Leonardo Primavera: Writing, Methodology, Investigation, Formal analysis, Data curation, Conceptualization.

Data availability Data will be made available on request.

Declarations

Conflict of interest The authors declare no conflict of interest.

References

Ashmore P (2013) in Treatise on Geomorphology, edited by E. Wohl (Academic, New York, Vol. 9. Chap 17:289–312

Ashmore P (2009) Intensity and characteristic length of braided channel patterns. Can J Civ Eng 36:1656

Bristow CS, Best JL (1993) in Braided Rivers, edited by C. S. Bristow and J. L. Best (Geological Society, London, 1993), pp. 1–11

Paola C (1996) in Coherent Flow Structures. In: Ashworth PJ et al (eds) Open Channels. Wiley, Chichester, pp 705–723

Hundey EJ, Ashmore PE (2009) Length scale of braided river morphology. Water Resour Res 45:W08409

Castelltort S (2018) Empirical relationship between river slope and the elongation of bars in braided rivers: A potential tool for paleoslope analysis from subsurface data. Mar Pet Geol 96:544

Sapozhnikov V, Foufoula-Georgiou E (1995) Selfsimilar/self-affine objects via logarithmic correlation integral. J Phys A: Math Theor 28:559

Sapozhnikov V, Foufoula-Georgiou E (1996) Self-affinity in braided rivers. Water Resour Res 32:1429

Sapozhnikov VB, Foufoula-Georgiou E (1997) Evidence of scaling and SOC in braided rivers. Water Resour Res 33(8):1983

Sapozhnikov V et al (1998) Validation of braided-stream models: scaling, island shapes. Water Resour Res 34:2353

Bassler KE, Paczuski M (1998) Simple model of superconducting vortex avalanches. Phys Rev Lett 81:3761

Bassler KE, Paczuski M, Reiter GF (1999) Braided rivers and superconducting vortex avalanches. Phys Rev Lett 83:3956

Sapozhnikov VB, Foufoula-Georgiou E (1999) Horizontal and Vertical Self-organization of braided rivers. Water Resour Res 35(3):843

Foufoula-Georgiou E, Sapozhnikov V (2001) Scale invariances in the morphology and evolution of braided rivers. Math Geol 33:273

Walsh J, Hicks D (2002) Braided channels: Self-similar or self-affine? Water Resour Res 38:18–1

De Bartolo SG, Primavera L, Gaudio R, D'Ippolito A, Veltri M (2006) Fixed-mass multifractal analysis of river networks and braided channels. Phys Rev E 74:026101

De Bartolo S, Fallico C, Ferrari E (2015) Simple scaling analysis of active channel patterns in Fiumara environment. Geomorphology 232:94

De Bartolo S et al (2022) Scaling behaviour of braided active channels: A Taylor's power law approach. Eur Phys J Plus 137:622

Stecca G, Hicks DM (2022) Numerical simulations of confined braided river morphodynamics. J Geophys Res Earth Surf 127:20210e2021JF006409

Taylor LR (1961) Aggregation, Variance and the Mean. Nature 189:732–735

Taylor RAJ (2019) Taylor's power law, order and pattern in nature. Academic Press, Cambridge

De Bartolo S (2024) Singularities of Taylor's power law in the analysis of aggregation measures. Physica A 654:130151

Rizzello S et al (2024) Multiscaling behavior of braided channel networks: An alternative formulation of Taylor's law variate transformations. Phys Rev E 109:034306

De Bartolo S, De Michele C (2025) Braiding as branching at the channel scale: a direct approach to network scaling. Eur Phys J Plus 140:668

De Michele C, Primavera L, Tomasicchio GR, Lauria A, Francone A, Leone E, Salvadori G, De Bartolo S (2025) Multifractal analysis of braided channel networks using structure functions and fixed-mass measures. Phys A Phys A 675:130831

Hurst HE (1951) Long-term storage capacity of reservoirs. Trans Am Soc Civ Eng 116:770–799

Mandelbrot BB, Wallis JR (1968) Noah, Joseph, and operational hydrology. Water Resour Res 4(5):909–918

Mandelbrot BB, Wallis JR (1969) Some long-run properties of geophysical records. Water Resour Res 5(2):321–340

Mandelbrot BB (1982) The Fractal Geometry of Nature. W. H. Freeman and Company, New York

Feder J (1988) Fractals. Plenum Press, New York

Mandelbrot BB, van Ness JW (1968) Fractional Brownian motions, fractional noises and applications. SIAM Rev 10:422–437

Mandelbrot BB (1985) Self-affine fractals and fractal dimension. Phys Scr 32:257–260

Kendal WS, Jørgensen B (2011) Tweedie convergence: a mathematical basis for Taylor's power law, 1/ f noise, and multifractality. Phys Rev E 84:066120

Kantelhardt JW, Koscielny-Bunde E, Rego HHA, Havlin S, Bunde A (2001) Detecting long-range correlations with detrended fluctuation analysis. Phys A 295:441–454

Kantelhardt JW, Zschiegner SA, Koscielny-Bunde E, Havlin S, Bunde A, Stanley HE (2002) Multifractal detrended fluctuation analysis of nonstationary time series. Phys A 316:87–114
Makaske B (2001) B, Anastomosing rivers: A review of their classification, origin and sedimentary products. Earth Sci Rev 53(3–4):149–196
Sarma JN (2005) Fluvial process and morphology of the Brahmaputra River in Assam. India Geomorphol 70(3–4):226–256
Latrubesse EM (2008) Patterns of anabranching channels: The ultimate end-member adjustment of mega rivers. Geomorphology 101(1–2):130–145
Best JL, Ashworth PJ, Mosselman E, Sarker MH, Roden JE (2022) The Jamuna-Brahmaputra River, Bangladesh. In: Gupta A (ed) Large Rivers: Geomorphology and Management. Wiley, Blackwell, pp 579–640
Nandi KK, Pradhan C, Dutta S, Khatua KK (2023) Identifying the stability trajectory of a large braided Brahmaputra River using a reach-scale process-based approach. J Hydrol 626(Part B):130329
Nelson A, Dudill A, Amin MR (2025) Timescales of formative discharge and principal controls on the channel width of the Jamuna River. Bangladesh Earth Surf Proces Landforms 50(15):e70212
Sarker MH, Thorne CR (2006) Morphological response of the Brahmaputra–Padma–Lower Meghna River system to the Assam earthquake of 1950, In G. H. Sambrook Smith, J. L. Best, C. S. Bristow, and G. Petts (Eds.), Braided Rivers: Process, Deposits, Ecology and Management (Special Publication of the International Association of Sedimentologists, No. 36, pp. 289–310), Blackwell, Oxford
Oświęcimka P, Kwapień J, Drożdż S (2006) Wavelet versus detrended fluctuation analysis of multifractal structures. Phys Rev E 74:016103
Kantelhardt JW (2011) Fractal and multifractal time series, in *Encyclopedia of Complexity and Systems Science*, Springer
Harris TE (1989) The Theory of Branching Processes. Dover Publications Inc, New York
Jensen HJ (1998) Self-Organized Criticality, Cambridge Lecture Notes in Physics
Bak P, Tang C, Wiesenfeld K (1987) Self-Organized Criticality: an explanation of $1/f$ noise. Phys Rev Lett 59(4):381–384
Bak P, Tang C, Wiesenfeld K (1988) Self-Organized Criticality. Phys Rev A 38(1):364–374
Mandelbrot BB (1986) In Fractals. In: Pietronero L, Tosatti E (eds) Physics. North-Holland, Amsterdam, pp 3–15
Badii R, Politi A (1984) Hausdorff dimension and uniformity factor of strange attractors. Phys Rev Lett 52:1661
Badii R, Politi A (1985) Statistical description of attractors: the dimension function. J Stat Phys 40:725
Bacry E, Muzy JF, Arneodo A (1993) Singularity spectrum of fractal signals from wavelet analysis: exact results. J Stat Phys 70:635
Muzy JF, Bacry E, Arneodo A (1993) Multifractal formalism for fractal signals: the structure-function approach versus the wavelet-transform modulus-maxima method. Phys Rev E 47:875
Pesin YB (1997) Dimension theory in dynamical systems. The University of Chicago Press, Chicago
Rizzello S, Scaraggi M, Nelson AD, Primavera L, Napoli G, Stecca G, Vitolo R, De Bartolo S (2023) Software and Dataset (Aggegation, Variance and Mean in Braided Channel Networks), Zenodo depository, available at https://doi.org/10.5281/zenodo.10104612
Sah RK, Das AK (2018) Morphological Dynamics of the Rivers of Brahmaputra. J Geol Soc India 92:381–510
Gogoi P (2018) Landscape evolution modelling in large, complex braided river: a case study of Majuli Island, North-East India, Ph.D. Thesis, University of Nottingham,
Singh VP, Sharma N, Ojha CSP (2004) The Brahmaputra Basin Water Resources. Kluwer Academic Publishers, Dordrecht
Lahiri SK (2023) The Brahmaputra River in Assam. Taylor & Francis, CRC Press
Egozi R, Ashmore P (2009) Experimental analysis of braided channel pattern response to increased discharge. J Geophys Res 114:F02012. https://doi.org/10.1029/2008JF001099
Bertoldi W, Zanoni L, Tubino M (2009) Planform dynamics of braided streams. Earth Surf Process Landforms 34(4):547–557. https://doi.org/10.1002/esp.1755
Ashmore P (2009) Intensity and characteristic length of braided channel patterns. Can J Civ Eng 36(10):1656–1666. https://doi.org/10.1139/L09-088